# Anomalous Electrodeposition of Metallic Mn Nanostructured Films on H-Terminated Si(100) at Anodic Potential

L. Y. Zhao, A. C. Siu, and K. T. Leung*

*WATLab and Department of Chemistry, University of Waterloo, Waterloo, Ontario N2L 3G1, Canada*

*Received July 10, 2007. Revised Manuscript Received October 10, 2007*

Electrodeposition of metallic Mn films onto H-terminated Si(100) from a solution of 10 mM $MnCl_2$ and 2 M $NH_4Cl$ is studied by linear sweep voltammetry over three different potential ranges (0 to −3.0 V, −3.0 to 1.5 V, and 0 to 1.5 V). Scanning electron microscopy shows that the formation of dendritic nanostructured films on H-terminated Si(100) occurs only in the positive potential range. X-ray photoelectron spectroscopy reveals that these films consist of metallic Mn covered by $Mn_7O_{13}$ hydrates and pyrolusite ($\beta$-$MnO_2$) as a minor surface component. Glancing-incidence X-ray diffraction shows that the $Mn_7O_{13}$ hydrate features are of the hexagonal phase, while the metallic Mn is amorphous. A plausible mechanism involving the reduction of $Mn^{2+}$ to metallic Mn along with the oxidation of Si to $SiO_x$ on the H-terminated Si(100) substrate is proposed to account for the observed anomalous anodic electrodeposition of metallic Mn. Furthermore, by annealing the resulting metallic Mn film at 600 °C in $N_2$, a mixture of manganese silicides (MnSi and $MnSi_{\sim 1.7}$) covered by manganese silicate ($Mn_2SiO_4$) is formed. Increasing the annealing temperature to 1000 °C significantly reduces the amount of silicate, and MnSi appears to have completely converted to $MnSi_{\sim 1.7}$.

## 1. Introduction

The study of thin metallic films deposited on Si substrates and their interfaces is important to both microelectronic and optoelectronic applications. The Mn–Si system has attracted increasing attention due to the formation of a variety of manganese silicides on the Si substrate. For example, $Mn_5Si_3$ is known to have complex and interesting magnetic properties.[1,2] MnSi is a weak intermetallic itinerant ferromagnet that exhibits a helical spin structure at its critical temperature $T_c$ slightly below 30 K.[3] $MnSi_{\sim 1.7}$ is a thermoelectric material appropriate for high-temperature applications due to its refractory and semiconducting properties,[4] and its optical properties also make it a promising candidate for Si-based optoelectronic devices.[5,6] To date, not much work has been reported on metallic Mn film growth on Si substrates, except for those prepared by vacuum deposition methods on Si(111)[7–15] and Si(100).[5,16–21] In the case of Mn film growth on Si(100), Lian and Chen prepared epitaxial $MnSi_{1.7}$ on Si(100) by two-step annealing of an electron-beam-evaporated Mn film (at 300 °C and then at 1000–1100 °C).[5] Bost and Mahan obtained polycrystalline $MnSi_{1.7}$ by ion-sputtering a thin layer of metallic Mn onto Si(100) followed by annealing at 1000 °C in Ar.[16] Zhang and Ivey obtained a mixture of $MnSi_{1.73}$ and MnSi by solid-phase reaction that involved annealing a thermally evaporated metallic Mn film on Si(100) at 485–570 °C in $N_2$.[17] Lippitz et al. reported that annealing an unstructured Mn film thermally evaporated on Si(100)(2 × 1) at 450 °C produced pancake-stack-like MnSi islands and hut-like $Mn_5Si_3$ islands.[18] Krause et al. observed the formation of three-dimensional $Mn_xSi_y$ islands upon annealing an unstructured Mn film on Si(100) to 300–700 °C.[19] Unlike these solid-phase reaction methods, Teichert et al. found that depositing Mn by electron-beam evaporation onto Si(100)(2 × 1) with the substrate held at an elevated temperature (reactive deposition) led only to the formation of polycrystalline $MnSi_{1.7}$.[20] Hou et al. reported

* Corresponding author. E-mail: tong@uwaterloo.ca.

(1) Irizawa, A.; Yamasaki, A.; Okazaki, M.; Kaasi, S.; Sekiyama, A.; Imada, S.; Suga, S.; Kulatov, E.; Ohta, H.; Nanba, T. *Solid State Commun.* **2002**, *124*, 1.
(2) Ramos Silva, M.; Brown, P. J.; Forsyth, J. B. *J. Phys.: Condens. Matter* **2002**, *14*, 8707.
(3) Ishikawa, Y.; Tajima, K.; Bloch, D.; Roth, M. *Solid State Commun.* **1976**, *19*, 525.
(4) Kawasumi, I.; Sakata, M.; Nishida, I.; Masumoto, K. *J. Mater. Sci.* **1981**, *16*, 355.
(5) Lian, Y. C.; Chen, L. J. *Appl. Phys. Lett.* **1986**, *48*, 359.
(6) Rebien, M.; Henrion, W.; Angermann, H.; Teichert, S. *Appl. Phys. Lett.* **2002**, *81*, 22.
(7) Evans, M. M. R.; Glueckstein, J. C.; Nogami, J. *Phys. Rev. B* **1996**, *53*, 4000.
(8) Shivaprasad, S. M.; Anandan, C.; Azatyan, S. G.; Gavriljuk, Y. L.; Lifshits, V. G. *Surf. Sci.* **1997**, *382*, 258.
(9) Nagao, T.; Ohuchi, S.; Matsuoka, Y.; Hasegawa, S. *Surf. Sci.* **1999**, *419*, 134.
(10) Zhang, Q.; Tanaka, M.; Takeguchi, M.; Furuya, K. *Surf. Sci.* **2002**, *507–510*, 453.
(11) Adambaev, K.; Yusupov, A.; Yakubov, K. *Inorg. Mater.* **2003**, *39*, 942.
(12) Kumar, A.; Tallarida, M.; Hansmann, M.; Starke, U.; Horn, K. *J. Phys. D* **2004**, *37*, 1083.
(13) Azatyan, S. G.; Iwami, M.; Lifshits, V. G. *Surf. Sci.* **2005**, *589*, 106.
(14) Ctistis, G.; Deffke, U.; Schwinge, K.; Paggel, J. J.; Fumagalli, P. *Phys. Rev. B* **2005**, *71*, 035431.
(15) Wang, H.; Zou, Z. Q. *Appl. Phys. Lett.* **2006**, *88*, 103115.
(16) Bost, M. C.; Mahan, J. E. *J. Electron. Mater.* **1987**, *16*, 389.
(17) Zhang, L.; Ivey, D. G. *J. Mater. Sci.: Mater. Electron.* **1991**, *2*, 116.
(18) Lippitz, H.; Paggel, J. J.; Fumagalli, P. *Surf. Sci.* **2005**, *575*, 307.
(19) Krause, M. R.; Stollenwerk, A.; Licurse, M.; LaBella, V. P. *J. Vac. Sci. Technol. A* **2006**, *24*, 1480.
(20) Teichert, S.; Schwendler, S.; Sarkar, D. K.; Mogilatenko, A.; Falke, M.; Beddies, G.; Kleint, C.; Hinneberg, H.-J. *J. Cryst. Growth* **2001**, *227–228*, 882.
(21) Hou, Q. R.; Wang, Z. M.; He, Y. J. *Appl. Phys. A: Mater. Sci. Process.* **2005**, *80*, 1807.

10.1021/cm071817v CCC: $37.00 © 2007 American Chemical Society
Published on Web 11/20/2007

MnSi and $MnSi_{1.7}$ films on Si(100) substrates synthesized by both solid-phase reaction and reactive deposition.[21,22]

Despite being a simple, low-cost, high-throughput fabrication technique, electrodeposition is not the method of choice for producing Mn films on a substrate. This is because Mn has a large negative reduction potential of $E^0(Mn^{2+}/Mn) = -1.40$ V (Ag/AgCl), making deposition of metallic Mn by electrochemical methods very difficult. Of the limited successful electrodeposition of metallic Mn reported to date, it appears essential to use a high cathodic potential on a selected few cathodes, including stainless steel and Ti electrode,[23,24] vitreous C disk, and Cu microelectrode.[25] In particular, Lewis et al. reported the electrodeposition of metallic Mn on a stainless steel and a Ti cathode in a $MnCl_2$ and $NH_4Cl$ solution with and without Se-based additives.[23,24] Gonsalves and Pletcher investigated the electrodeposition of metallic Mn onto vitreous C disk electrode and Cu microelectrode by potential step techniques from −1.30 V to −1.63 to −1.67 V in an aqueous solution of $MnCl_2$ and $NH_4Cl$.[25] Gong and Zangaria deposited metallic Mn on a stainless steel substrate in a solution of $MnSO_4$ and $(NH_4)_2SO_4$ (with and without the addition of small amounts of $SnSO_4$ or $CuSO_4$) by potentiodynamic scans and the galvanostatic method at −1.5 to −2.5 V in wide ranges of pH and current density.[26,27] Recently, Díaz-Arista et al. studied metallic Mn electrodeposition on a Fe-covered quartz crystal in a solution of $MnCl_2$, $H_3BO_3$, and KCl (with and without the use of a $NH_4SCN$ additive) by cyclic voltammetry and the potentiostatical method in an electrochemical quartz crystal microbalance, with the deposition potential more cathodic than −1.5 V.[28] To date, no successful electrodeposition of metallic Mn on a Si substrate (at any deposition potential) has been reported. In the present work, we report the formation of metallic Mn films onto a H-Si(100) (i.e., H-terminated) substrate by electrochemical deposition for the first time and only at an anodic potential. A simple mechanism involving oxidation of Si to $SiO_2$ and reduction of $Mn^{2+}$ to metallic Mn on the H-Si(100) substrate is proposed to explain this anomalous electrodeposition.

## 2. Experimental Details

Details of our three-electrode cell setup and procedures for the electrodeposition experiments have been given elsewhere.[29] Briefly, the working electrodes were single-side-polished rectangular (15 × 2.5 $mm^2$) p-type Si(100) chips (0.4 mm thick), with a resistivity of 1.0–1.5 mΩ cm, that have been H-terminated by using a standard procedure.[30] A standard Ag/AgCl electrode was used as the reference electrode while a Pt wire was used as the counter electrode. In a deoxygenated aqueous solution of 10 mM $MnCl_2$ and 2 M $NH_4Cl$, Mn was deposited on the H-Si(100) substrate by cyclic voltammetry, linear sweep voltammetry over different ranges of applied potential, and potentiostatic amperometry. After the deposition, the Si substrate was thoroughly rinsed with Millipore water and dried in $N_2$ before further analysis. The surface morphology of the Mn deposits was characterized by field emission scanning electron microscopy (SEM), while their corresponding chemical state and composition were studied by X-ray photoelectron spectroscopy (XPS) as a function of sputtering depth. Charge neutralization was found to be necessary during the XPS analysis, and the resulting binding energies of C 1s and Si $2p_{3/2}$ (for the elemental Si) upon charge compensation were found to be respectively 284.6 and 99.1 eV, in good accord with the literature values. Argon sputtering was performed over a rastered area of 3 × 3 $mm^2$ of the sample at an ion beam energy of 3 keV and an average ion current density of 122 nA $mm^{-2}$. The crystal structure of the deposits was characterized by glancing-incidence X-ray diffraction (GIXRD) with the Cu Kα anode operating at 45 kV and 40 mA.

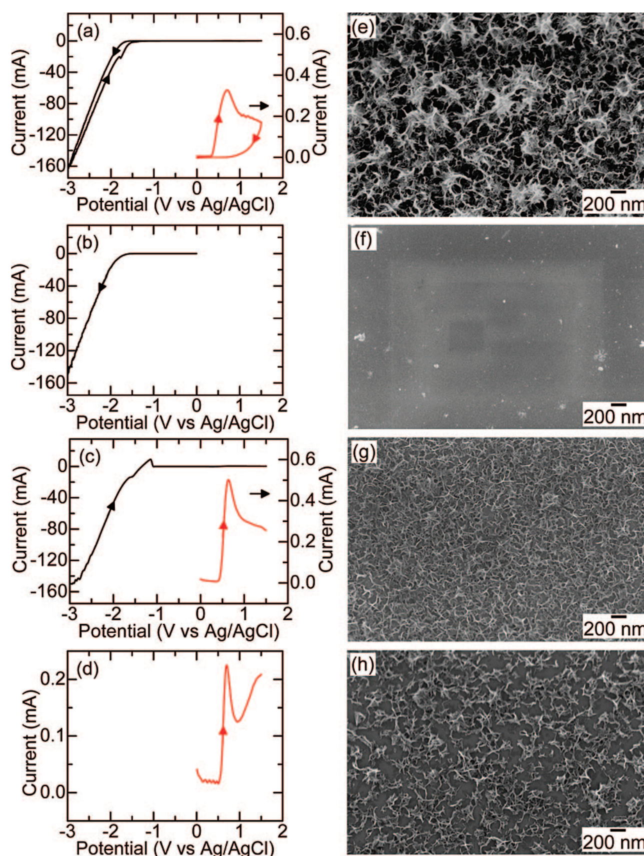


**Figure 1.** (a) Cyclic voltammogram and linear sweep voltammetric scans (b) from 0 to −3.0 V, (c) from −3.0 to 1.5 V, and (d) from 0 to 1.5 V for H-Si(100) in a solution of 10 mM $MnCl_2$ and 2 M $NH_4Cl$, all at a potential scan rate of 0.01 V $s^{-1}$. The arrows on the curves indicate the scan directions. For (a) and (c), an exploded view of the respective curve above 0 V is shown with an expanded scale depicted on the right *y*-axis. The corresponding SEM images of the resulting Mn films deposited on H-Si(100) are shown in (e), (f), (g), and (h), respectively.

## 3. Results and Discussion

Figure 1a shows a typical cyclic voltammogram recorded at a potential scan rate of 0.01 V $s^{-1}$ for Mn electrodeposits on H-Si(100) in a solution of 10 mM $MnCl_2$ and 2 M $NH_4Cl$. Evidently, in the forward scan from 0 to −3.0 V, essentially


(22) Wang, Z. M.; Hou, Q. R.; He, Y. J. *Mod. Phys. Lett. B* **2002**, *16*, 583.
(23) Lewis, J. E.; Scaife, P. F.; Swinkels, D. A. *J. Appl. Electrochem.* **1976**, *6*, 199.
(24) Lewis, J. E.; Scaife, P. F.; Swinkels, D. A. *J. Appl. Electrochem.* **1976**, *6*, 453.
(25) Gonsalves, M.; Pletcher, D. *J. Electroanal. Chem.* **1990**, *285*, 185.
(26) Gong, J.; Zangari, G. *J. Electrochem. Soc.* **2002**, *149*, C209.
(27) Gong, J.; Zangari, G. *Electrochem. Solid State Lett.* **2004**, *7*, C91.
(28) Díaz-Arista, P.; Antaño-López, R.; Meas, Y.; Orteg, R.; Chainet, E.; Ozil, P.; Trejo, G. *Electrochim. Acta* **2006**, *51*, 4393.
(29) Zhao, L. Y.; Eldridge, K. R.; Sukhija, K.; Jalili, H.; Heinig, N. F.; Leung, K. T. *Appl. Phys. Lett.* **2006**, *88*, 033111.
(30) Kern, W., Ed. *Handbook of Semiconductor Wafer Cleaning Technology*; Noyes: Park Ridge, 1993.

no current is observed until −1.65 V, after which the cathodic current increases sharply. In the backward scan from −3.0 to 1.5 V, an anodic peak at 0.69 V is clearly observed (in the exploded view shown with an enlarged current scale on the right *y*-axis). No feature is observed during the potential scan from 1.5 to 0 V. The corresponding SEM image of the resulting deposit, denoted as sample A (Figure 1e), reveals a highly convoluted dendritic structure. Energy-dispersive X-ray analysis (not shown) indicates that the Mn electrodeposits consist primarily of Mn, C, and O. To further investigate these nanostructured films, we performed on fresh H-Si(100) substrates linear sweep voltammetric deposition over three different voltage ranges: (sample B) from 0 to −3.0 V (Figure 1b), (sample C) from −3.0 to 1.5 V (Figure 1c), and (sample D) from 0 to 1.5 V (Figure 1d). Samples B and C may be regarded as the deposition obtained by the forward and backward scans, respectively, of the cyclic voltammogram (sample A), while sample D corresponds to the anodic part of the deposition for sample C. Evidently, no discernible deposit is found for sample B obtained by cathodic deposition, and the observed SEM image (Figure 1f) corresponds essentially to the Si substrate. The SEM image of sample C (Figure 1g) resembles that of the electrodeposits obtained by cyclic voltammetry (Figure 1e), except that the dendrites appear to be finer and considerably less dense. A similar SEM image for sample D (Figure 1h) with the dendrite density even lower than sample C but with a correspondingly larger number of bare substrate areas is observed. Even though the cathodic deposition does not appear to produce any discernible deposit on the H-Si(100) substrate for sample B, the defect density of the surface could be increased, resulting in a higher number density of island growth and consequently more dendrites in sample C than sample D. For samples B and C that involve cathodic deposition, formation of a brown film corresponding to manganese oxide ($Mn_xO_y$) on the Pt counter electrode (anode) is also observed, as expected from the anodic deposition.

Figure 2 compares the respective Mn 2p XPS spectra for samples B, C, and D. For sample B, the survey spectrum (Figure 2a) shows XPS features attributable to C, O, and Si and confirms that no Mn 2p feature is found. For samples C (Figure 2b) and D (Figure 2c), the Mn 2p XPS spectra for the as-deposited films and the corresponding depth profiles are found to be very similar to each other. It should be noted that the film thickness of sample C is larger than that of sample D, as indicated by the area ratios of the Mn $2p_{3/2}$ and Si 2p peaks for the as-deposited sample C (42.0) and sample D (5.9). For both as-deposited samples, the peak shape and position of the prominent Mn $2p_{3/2}$ ($2p_{1/2}$) feature at 642.4 eV (654.0 eV) are characteristic of that reported for pyrolusite ($\beta$-$MnO_2$).[31] Upon sputtering for 10–15 s, the $\beta$-$MnO_2$ feature at 642.4 eV (654.0 eV) has evidently been removed, and the prominent Mn $2p_{3/2}$ ($2p_{1/2}$) feature can be fitted with two components arising from MnO at 640.7 eV (652.2 eV) and $\epsilon$-$MnO_2$ at 641.6 eV (653.5 eV).[32,33] The

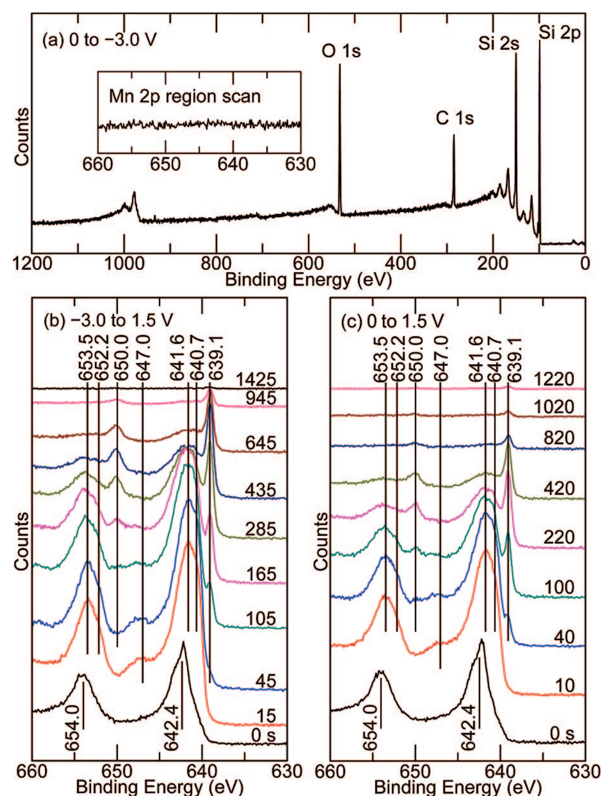


**Figure 2.** (a) Survey XPS spectrum and Mn 2p region scan (inset) of Mn deposition on H-Si(100) from a solution of 10 mM $MnCl_2$ and 2 M $NH_4Cl$ by linear sweep voltammetric scan from 0 to −3.0 V. Depth-profiling XPS spectra of Mn 2p region for the corresponding Mn deposition obtained by voltammetric scan (b) from −3.0 to 1.5 V and (c) from 0 to 1.5 V.

weak feature emerging at 647 eV (i.e., ~6 eV above the main Mn $2p_{3/2}$ photopeak) is characteristic of a shakeup feature of $Mn^{2+}$ ion (MnO), in accord with the work reported by Di Castro and Polzonetti.[34] It should be noted that the observed binding energy value of Mn $2p_{3/2}$ for MnO (640.7 eV) is found to be in excellent accord with those reported in the literature (640.7 and 640.9 eV).[32,33] The Mn $2p_{3/2}$ binding energy value for $\epsilon$-$MnO_2$ (641.6 eV) is identical to that obtained for a commercial $\epsilon$-$MnO_2$ powder measured separately by us (not shown) and to that reported by Colmenares et al. (641.7 eV).[33] Further sputtering for >40 s reveals a sharp Mn $2p_{3/2}$ ($2p_{1/2}$) feature at 639.1 eV (650.0 eV) attributable to metallic Mn.[35] Continued sputtering to 600 s reduces the Mn oxide features, and only the metallic Mn features remain after 800 s of sputtering. The corresponding depth-profiling O 1s XPS spectra for samples C and D are also shown in Figure 3. Before sputtering, the O 1s feature at 529.8 eV corresponds to the surface $\beta$-$MnO_2$[31] while the nature of the other broad feature near 532 eV is generally complex, and it could have contributions from different types and amounts of Si oxides[36] (as confirmed by

(31) Ramstedt, M.; Shchukarev, A. V.; Sjöberg, S. *Surf. Interface Anal.* **2002**, *34*, 632.
(32) Słoczyński, J.; Grabowski, R.; Kozłowska, A.; Olszewski, P. K.; Stoch, J. *Phys. Chem. Chem. Phys.* **2003**, *5*, 4631.
(33) Colmenares, C.; Deutsch, S.; Evans, C.; Nelson, A. J.; Terminello, L. J.; Reynolds, J. G.; Roos, J. W.; Smith, I. L. *Appl. Surf. Sci.* **1999**, *151*, 189.
(34) Di Castro, V.; Polzonetti, G. *J. Electron Spectrosc. Relat. Phenom.* **1989**, *48*, 117.
(35) Moulder, J. F.; Stickle, W. F.; Sobol, P. E.; Bomben, K. D. *Handbook of X-ray Photoelectron Spectroscopy*, 2nd ed.; Chastain, J., Ed.; Perkin-Elmer Corp.: Eden-Prairie, MN, 1992.
(36) Wu, J. X.; Ma, M. S.; Zheng, H. G.; Yang, H. W.; Zhu, J. S.; Ji, M. R. *Phys. Rev. B* **1999**, *60*, 17102.

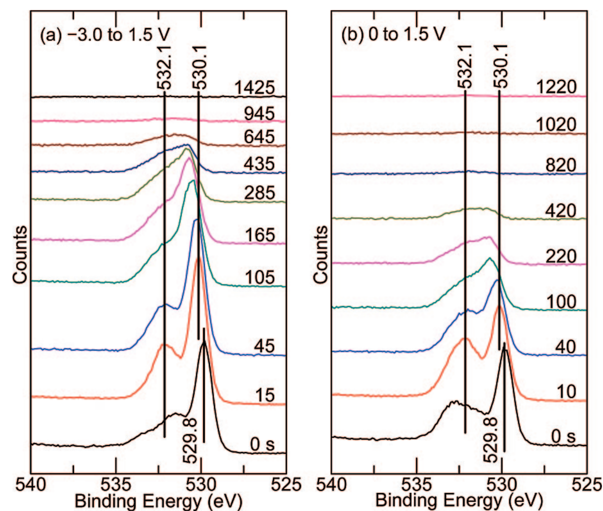


**Figure 3.** Depth-profiling XPS spectra of O 1s region for the corresponding Mn deposition on H-Si(100) from a solution of 10 mM $MnCl_2$ and 2 M $NH_4Cl$ by linear sweep voltammetric scan (a) from −3.0 to 1.5 V and (b) from 0 to 1.5 V.

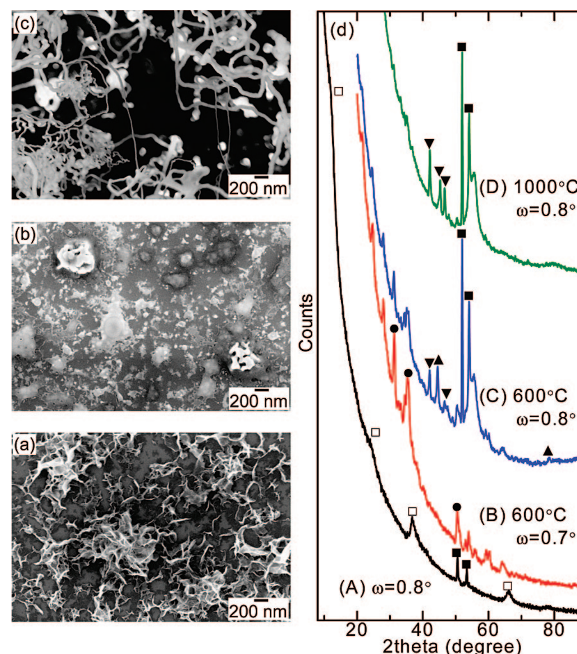


**Figure 4.** SEM images of Mn film (a) as-deposited on H-Si(100) from a solution of 10 mM $MnCl_2$ and 2 M $NH_4Cl$ at 1.5 V for 40 min and upon annealing for 4 h in $N_2$ at (b) 600 °C and (c) 1000 °C. The corresponding GIXRD patterns (collected at the respective incidence angle $\omega$) of the Mn film (A) as-deposited, and upon the anneals at (B, C) 600 °C and (D) 1000 °C are shown in (d). The symbols ■, □, ●, ▼, and ▲ identify the diffraction features from Si, $Mn_7O_{13}\cdot5H_2O$, $Mn_2SiO_4$, $MnSi_{\sim1.7}$, and MnSi, respectively.

the Si 2p feature at ~103 eV—not shown) and from surface water molecules.[37] After brief sputtering for 10–15 s, a well-defined O 1s feature emerges at 530.1 eV, and it can be attributed to $Mn_7O_{13}$ (as discussed below). Concomitantly, the higher binding energy feature near 532 eV becomes sharper, and it can be assigned to silicon suboxide ($SiO_x$)[36] and to the water of crystallization in $Mn_7O_{13}\cdot5H_2O$ (as also shown by our GIXRD result below). The apparent shift in the maximum of the O 1s envelop is due to the reported shift of the O 1s feature of $SiO_x$ to a lower binding energy with increasing sputtering time.[38] It may be possible that there is interaction at the Mn–Si interface and that the Mn–silicide may already exist at room temperature.[12,39] However, regardless of whether Mn–silicide is present or not, there must still be metallic Mn on the surface Si (as indicated by the Mn 2p feature at 639.1 eV). If there is only Mn–silicide (which is stable in air to a high temperature), annealing such a sample in air would not produce Mn–silicate.

The corresponding depth-profiling Si 2p XPS spectra for samples C and D are also very similar (not shown). Before sputtering, the two features at 99.1 and 99.7 eV correspond respectively to the Si $2p_{3/2}$ and $2p_{1/2}$ components of elemental Si, while the weaker broad feature at 103.1 eV can be attributed to Si 2p of silicon suboxide ($SiO_x$). Upon sputtering for 1425 s, the surface silicon suboxide is removed, and only the elemental Si components remain. It should be noted that the reaction between Mn and Si could induce a binding energy shift of 0.15–0.18 eV to the lower binding energy in Si 2p.[12,39] Unlike synchrotron radiation sources, it is difficult for the present XPS setup to discern such a small shift with a monochromatized laboratory X-ray source, despite the achievable energy resolution.

In separate experiments, we also performed cathodic electrodeposition on H-Si substrates at several negative potentials including −1.4, −1.6, and −1.8 V, each for 100 s. A brown film corresponding to manganese oxide ($Mn_xO_y$) was observed on the Pt counter electrode (anode), while no deposition on the H-Si substrate (cathode) was found from the corresponding SEM or XPS analyses (not shown). It should be noted that the deposition times in these experiments were chosen to be short intentionally to avoid severe hydrolysis that would occur at a longer cathodic electrodeposition time. Furthermore, we also conducted anodic electrodeposition on H-Si substrates at several positive potentials including 0, 0.5, 1.0, and 1.5 V, each for 20 min. The respective SEM studies showed that there was no deposition for the samples obtained at 0 and 0.5 V, while dendrite structures on the H-Si substrate were found for the samples deposited at 1.0 and 1.5 V. The corresponding depth-profiling XPS spectra for these latter samples (not shown) were found to be very similar to those of sample C (obtained by voltammetric scan from −3.0 to 1.5 V) and sample D (obtained from 0 to 1.5 V) (Figure 3). These experiments therefore conclusively show that metallic Mn can only be obtained by anodic deposition.

In order to better characterize the crystallography of the Mn film, we prepared a Mn film with a sufficient thickness for GIXRD measurement by electrodeposition at a fixed anodic potential of 1.5 V for 40 min. As expected, the morphology of the as-deposited Mn film (Figure 4a) is similar to that of sample D discussed earlier (Figure 1h). Subsequent XPS depth profiling experiments (not shown) confirm the presence of metallic Mn in the resulting film. The corresponding GIXRD pattern of the as-deposited film

(37) Kim, Y. J.; Gao, Y.; Chambers, S. A. *Appl. Surf. Sci.* **1997**, *120*, 250.
(38) Torchinskaya, T. V.; Korsunskaya, N. E.; Khomenkova, Yu. L.; Dhumaev, B. R.; Prokes, S. M. *Thin Solid Films* **2001**, *381*, 88.
(39) Magnano, E.; Carleschi, E.; Nicolaou, A.; Pardini, T.; Zangrando, M.; Parmigiani, F. *Surf. Sci.* **2006**, *600*, 3932.

shown in Figure 4d depicts two sharp features at 50.5° and 53.5° (identified by ■ on curve A) corresponding to the (311) plane of Si.[40] The broader features at 12.3°, 24.4°, 36.9°, and 66.5° (□ on curve A) can be assigned to surface oxide $Mn_7O_{13}\cdot5H_2O$ (JCPDS 23-1239),[41,42] and the generally large widths of these features further suggest that the oxide is poorly crystalline. The positive GIXRD identification of surface oxide $Mn_7O_{13}\cdot5H_2O$ is in good accord with our XPS analysis (Figures 2 and 3). No GIXRD features attributable to the surface $\beta$-$MnO_2$ can be observed, which suggests that its amount is likely too small to be detectable. The present pattern also does not reveal any metallic Mn feature as previously identified by the sharp Mn $2p_{3/2}$ ($2p_{1/2}$) feature at 639.1 eV (650.0 eV) in Figure 2, which suggests that the metallic Mn is amorphous. Annealing the as-deposited film at 600 °C for 4 h in $N_2$ was found to produce remarkably different GIXRD patterns (curves B and C). All the features in the GIXRD pattern collected at $\omega = 0.7°$ can be attributed to crystalline manganese silicate $Mn_2SiO_4$ (JCPDS 89-7714). For instance, the three strongest lines at 31.2°, 35.0°, and 50.3° (● on curve B) can be assigned to the (301), (121), and (222) planes, respectively. At this small incidence angle, no evidence of the substrate Si peak is observed. At a slightly larger incidence angle ($\omega = 0.8°$) and hence with a larger X-ray penetration depth, the GIXRD pattern (curve C) as expected reveals the Si features at 51–58° corresponding to the (311) plane diffraction of the Si(100) substrate, similar to that observed for curve A. Curve C also contains all the corresponding $Mn_2SiO_4$ features found on curve B, but with additional manganese silicide features at 42.1° and 46–48° and at 44.5° and 78.4°, which can be attributed to tetragonal $MnSi_{\sim1.7}$ (▼ on curve C, JCPDS 89-2413) and cubic MnSi (▲ on curve C, JCPDS 42-1487), respectively. Furthermore, extending the annealing time of the as-deposited film at 600 °C in $N_2$ from 4 to 40 h does not lead to any discernible change in the GIXRD pattern (not shown), which suggests that a longer annealing time at 600 °C could not convert MnSi to $MnSi_{\sim1.7}$, and a 4 h anneal is already sufficient for the growth of manganese silicide. Since the annealing temperature could be a key controlling factor, we repeated the annealing experiment at 1000 °C but kept the annealing time at 4 h. The GIXRD pattern of the resulting sample (curve D) also reveals the very weak features due to $Mn_2SiO_4$ and the intense Si(100) substrate features. Furthermore, the features due to MnSi appear to have disappeared and only the $MnSi_{\sim1.7}$ features (▼ on curve D) remain. The phase transition from MnSi to $MnSi_{\sim1.7}$ reported at higher annealing temperatures[17,43,44] suggests that MnSi has been converted to $MnSi_{\sim1.7}$ at 1000 °C in the present case. This annealing behavior is consistent with the earlier studies. In particular, Eizenberg and Tu deposited α-Mn on Si(100) by electron beam evaporation and found that annealing the sample to below 400 °C did not produce any interdiffusion but annealing at 400 °C generated MnSi, which underwent further reaction with Si to form $MnSi_{1.7}$ at 500 °C.[43] Zhang and Ivey observed that the ratio of $MnSi_{1.73}$ and MnSi could be increased by increasing the annealing temperature to 540 and 570 °C in $N_2$.[17] Wang et al. prepared MnSi and $MnSi_{1.7}$ by annealing a vacuum-deposited Mn film on Si(100) at 400 and 600 °C, respectively.[44] In contrast to the earlier studies that report complete conversion of MnSi to $MnSi_{\sim1.7}$ at 600 °C, we detect both MnSi and $MnSi_{\sim1.7}$ at this annealing temperature. This could be due to the higher level of impurities expected in the present (wet) electrochemical deposition technique than that in (dry) vacuum deposition because impurities can obstruct the silicide formation.[43]

SEM, energy-dispersive X-ray analysis, and XPS were also performed on the sample upon annealing at 600 and 1000 °C. The dendritic structure of the as-deposited film (Figure 4a) has evidently amalgamated to island-like aggregates (Figure 4b) and to nanowires (Figure 4c) after the 600 and 1000 °C anneals, respectively. Furthermore, the energy-dispersive X-ray analysis shows that the Mn-to-Si atomic ratio of the as-deposited sample appears to remain unchanged upon annealing at 600 °C ($1.76 \times 10^{-3}$) and to decrease at 1000 °C ($8.09 \times 10^{-4}$). The corresponding XPS spectra for both annealed samples (not shown) reveal the presence of surface $Mn_2SiO_4$, and the corresponding intensity ratio of Mn $2p_{3/2}$ (at 642.6 eV) to Si 2p (of the substrate) appears to decrease from 600 °C (0.70) to 1000 °C (0.10). These results suggest the decomposition of $Mn_2SiO_4$ at high temperature, but how $Mn_2SiO_4$ was decomposed and removed is not known.

In order to understand the mechanism of electrodeposition of metallic Mn on H-Si(100), we repeated the electrodeposition experiments using a single-side-polished float glass coated with 150–200 nm thick indium tin oxide (ITO) (with a sheet resistance of 4–8 Ω) as the working electrode, while keeping all the other deposition conditions the same. The inset of Figure 5a shows a linear voltammogram from 0 to 1.5 V recorded at a potential scan rate of 0.01 V $s^{-1}$, which clearly depicts the anodic peak at 1.1 V corresponding to the oxidation of $Mn^{2+}$ to $MnO_2$. Figure 5a shows the SEM image of the separate Mn film electrodeposited onto the ITO–glass substrate potentiostatically at 1.1 V for 600 s. The Mn film so obtained on ITO appears to have a similar, highly convoluted dendritic structure as that found for H-Si(100) (Figure 1). The corresponding GIXRD pattern of the as-deposited film (Figure 5b) is also found to be in good accord with crystalline hexagonal $Mn_7O_{13}\cdot5H_2O$ (JCPDS 23-1239). An XPS survey spectrum (not shown) of the as-deposited film reveals no evidence of In or Sn, indicating that the as-deposited film is continuous and thicker than the electron escape depth (estimated to be >2.2 nm). Depth-profiling analysis (Figure 5c) shows that the Mn $2p_{3/2}$ features corresponding to surface $\beta$-$MnO_2$ (at 642.4 eV) for the as-deposited film and to MnO (at 640.7 eV) and $\epsilon$-$MnO_2$ (at 641.6 eV) for the film upon sputtering. The shakeup feature at 647 eV (6 eV higher than the Mn $2p_{3/2}$ peak for MnO) observed upon sputtering is characteristic of $Mn^{2+}$. Continued sputtering of the deposited film does not reveal any Mn $2p_{3/2}$ feature assignable to metallic Mn, which indicates that

(40) Cho, B. O.; Chang, J. P.; Min, J. H.; Moon, S. H.; Kim, Y. W.; Levin, I. *J. Appl. Phys.* **2003**, *93*, 745.
(41) Giovanoli, R.; Stähli, E.; Feitknecht, W. *Helv. Chim. Acta* **1970**, *53*, 453.
(42) Chiganez, M.; Ishikawa, M. *J. Electrochem. Soc.* **2000**, *147*, 2246.
(43) Eizenberg, M.; Tu, K. N. *J. Appl. Phys.* **1982**, *53*, 6885.
(44) Wang, J. L.; Hirai, M.; Kusaka, M.; Iwami, M. *Appl. Surf. Sci.* **1997**, *113/114*, 53.

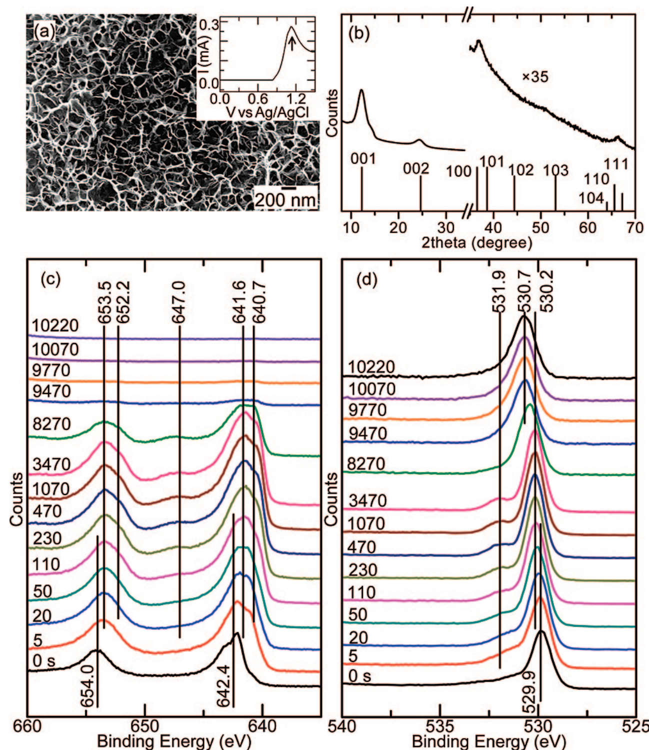


**Figure 5.** (a) SEM image; (b) GIXRD pattern; and XPS depth profiling spectra of (c) the Mn 2p and (d) O 1s regions for Mn electrodeposits on an ITO substrate from a solution of 10 mM $MnCl_2$ and 2 M $NH_4Cl$ at 1.1 V for 600 s. The inset in (a) shows the linear voltammogram (from 0 to 1.5 V) recorded at a potential scan rate of 0.01 V $s^{-1}$. The reference spectrum for $Mn_7O_{13}\cdot 5H_2O$ (JCPDS 23-1239) is also shown in (b).

the deposited film is predominantly $Mn_7O_{13}\cdot 5H_2O$. The corresponding O 1s XPS depth-profiling spectra are shown in Figure 5d. For the as-deposited sample, the prominent O 1s feature at 529.9 eV corresponds to the predominant surface $\beta$-$MnO_2$. With sputtering the O 1s feature appears to shift to 530.2 eV due to $Mn_7O_{13}$, while the weak feature at 531.9 eV could be attributed to the water of crystallization in $Mn_7O_{13}\cdot 5H_2O$. Further sputtering (>9770 s) eventually removes most of the deposited film, exposing the O 1s feature at 530.7 eV that can be assigned to the oxygen in the ITO substrate.[45] Evidently, only a $Mn_7O_{13}\cdot 5H_2O$ film can be obtained on an ITO substrate by anodic electrodeposition, in contrast to the H-Si(100) substrate where $Mn_7O_{13}\cdot 5H_2O$ is found on top of a metallic Mn film. Because $Mn_7O_{13}\cdot 5H_2O$ is present on the surfaces of the two as-deposited films, it is not surprising that both films exhibit similar morphology of dendritic structure. It should be noted that only Mn oxide was observed on ITO substrate while metallic Mn was found on the H-Si(100) substrate both by XPS depth profiling, which indicates that the observation of metallic Mn was not the consequence of the sputter-etch process. Furthermore, the XPS depth profiling spectra of commercial $MnO_2$ (not shown) also did not reveal any metallic Mn feature, which confirms that sputtering could not induce reduction of Mn oxide and generate metallic Mn.

Of all the studies reported to date, electrodeposition of metallic Mn (involving chloride or sulfate electrolytic solution) was found to occur only in a negative potential range, i.e., on the cathode such as Cu, vitreous C disk, stainless steel, and Ti electrodes.[23–28] On the other hand, manganese oxide is mostly obtained by potentiostatic or galvanostatic anodic electrodeposition onto an appropriate substrate (anode).[42,46] In the present work, we show for the first time that metallic Mn can be obtained on H-Si(100) and by anodic electrodeposition. To account for this anomalous anodic deposition observed for metallic Mn on the H-Si(100) substrate, we propose the following mechanism.

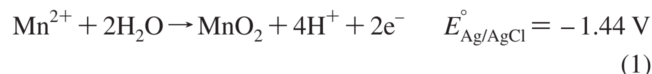

$$Mn^{2+} + 2H_2O \rightarrow MnO_2 + 4H^+ + 2e^- \qquad E^{\circ}_{Ag/AgCl} = -1.44\ V \tag{1}$$

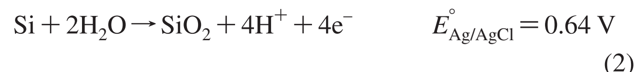

$$Si + 2H_2O \rightarrow SiO_2 + 4H^+ + 4e^- \qquad E^{\circ}_{Ag/AgCl} = 0.64\ V \tag{2}$$

$$Mn^{2+} + 2e^- \rightarrow Mn \qquad E^{\circ}_{Ag/AgCl} = -1.40\ V \tag{3}$$

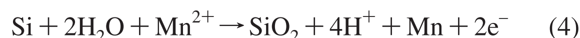

$$Si + 2H_2O + Mn^{2+} \rightarrow SiO_2 + 4H^+ + Mn + 2e^- \tag{4}$$

(It should be noted that the potentials for reactions 1 and 2 are not the "reduction" potentials. For clarity of the following discussion, we indicate the reaction potentials corresponding to the reactions as written.) At a negative potential, the Mn(II) reduction expected to proceed on the H-Si(100) working electrode (cathode) did not occur. Instead, the Mn(II) oxidation on the Pt counter electrode (anode) was observed. It can therefore be concluded that the Mn(II) oxidation on the Pt counter electrode competes with the Mn(II) reduction and simultaneous $H_2$ evolution on the H-Si(100) working electrode, resulting in the deposition of $Mn_xO_y$ on the Pt counter electrode without any metallic Mn deposition on the working electrode. As shown in Figure 1a, the sharp increase in the cathodic current after −1.65 V should be due to the evolution of $H_2$. Since hydrogen evolution is very strong on the working electrode, the local pH could increase, which would induce hydrolysis producing $Mn(OH)_2$. It should be noted that the presence of $Mn(OH)_2$ was confirmed by the appearance of brown precipitation in the solution during cathodic electrodeposition for a longer period of time. The deposition of $Mn_xO_y$ on Pt electrode and the formation of $Mn(OH)_2$ in the electrolyte solution therefore inhibit deposition on the H-Si substrate by cathodic electrodeposition. At a positive potential, dendritic nanostructured metallic Mn films are deposited (Figure 4a). The standard electrode potential for deposition of $MnO_2$ (eq 1) is −1.44 V vs Ag/AgCl, and the negative half-reaction potential indicates that the half-reaction is not spontaneous and requires energy to be supplied. Because the standard electrode potential of $SiO_2$ formation (eq 2) is 0.64 V vs Ag/AgCl, this half-reaction is spontaneous and therefore $SiO_2$ would be easily formed instead of $MnO_2$, releasing the electrons for the reduction of $Mn^{2+}$ to metallic Mn on the H-Si(100) working electrode (eq 3). Combining eqs 2 and 3 gives the overall half-cell reaction (eq 4), with a half-cell potential of −0.12 V, which means that the reaction from left to right is not spontaneous, thus requiring electrical work to force the reaction to the right. This is confirmed by the fact that simply dipping the

(45) Lägel, B.; Beerbom, M. M.; Doran, B. V.; Lägel, M.; Cascio, A.; Schlafa, R. *J. Appl. Phys.* **2005**, *98*, 023512.

(46) Córdoba de Torresi, S. I.; Gorenstein, A. *Electrochim. Acta* **1992**, *37*, 2015.

working electrode in the electrolyte (i.e., without applying any electrical work) would not produce any metallic Mn on the H-Si(100) substrate. In the case of the ITO substrate (Figure 5), however, the deposition at positive potential follows eq 1, which leads to the formation of $MnO_2$ as part of the crystalline $Mn_7O_{13}\cdot 5H_2O$ (i.e., $MnO\cdot 6MnO_2\cdot 5H_2O$).

## 4. Conclusion

Dendritic nanostructured metallic Mn film was electrodeposited onto H-Si(100) at a positive potential for the first time, providing a cost-effective method to prepare metallic Mn films on a Si substrate. XPS and GIXRD analyses indicate that the film consists of amorphous metallic Mn covered by poorly crystallized $Mn_7O_{13}$ hydrates with pyrolusite ($\beta$-$MnO_2$) as a minor surface component. We propose a plausible mechanism for the anodic electrodeposition of metallic Mn onto H-Si(100) that involves oxidation of Si to $SiO_2$ and reduction of $Mn^{2+}$ to metallic Mn on the H-Si(100) working electrode. The proposed mechanism can in principle be applicable to the deposition of other metals with a similar standard reduction potential $E^{o}$Ag/AgCl (e.g., V and Zr) on a H-terminated Si substrate. After annealing the as-deposited Mn film in $N_2$ at 600 °C for 4 h, the film was found to convert to polycrystalline manganese silicides $MnSi_{\sim 1.7}$ and MnSi covered by manganese silicate ($Mn_2SiO_4$). Because of the coexistence of metallic MnSi and semiconducting $MnSi_{\sim 1.7}$, it should be of great interest to further study the thermoelectric and magnetic properties of this sample. By increasing the annealing temperature to 1000 °C, the amount of $Mn_2SiO_4$ was significantly reduced, and MnSi was completely converted to $MnSi_{\sim 1.7}$.

**Acknowledgment.** This work is supported by the Natural Sciences and Engineering Research Council of Canada.

CM071817V